

Linear and Harmonic Magneto-dielectric Study on $\text{Ca}_3\text{Mn}_2\text{O}_7$ Layered Perovskite

Pooja Sahlot and A.M. Awasthi*

UGC-DAE Consortium for Scientific Research, University Campus, Khandwa Road, Indore- 452 001, India

Abstract: Dielectric study on $\text{Ca}_3\text{Mn}_2\text{O}_7$ features relaxor-like segmented dynamics below the antiferromagnetic ordering. Dipolar relaxations associated with rotation and tilt octahedral-distortions are spectrally resolved and their temperature-frequency dispersions exhibit distinct H -field alterations. This identifies their allegiance to different magnetic sub-phases and establishes dual coupling of electrical, magnetic, and structural degrees of freedom. Short-range electrical correlations— due to the randomness of structural distortions— collaterally cause measurable harmonic dielectric response in the system. The χ_3^e -susceptibility signal yields genuine harmonic magneto-dielectricity, consistent with but exhibiting two orders of magnitude larger H -field effect, vis-à-vis that obtained in the fundamental dielectric constant ϵ' .

Keywords: Layered Perovskite, Magneto-dielectricity, Non-linear Permittivity, Relaxor-like Vitreousity.

INTRODUCTION

Interesting evolution of magnetic and electrical configurations has been realized in layered Ruddlesden-Popper (R-P) compounds. These are pronounced successor of perovskites with inter-coupled structural, magnetic, and electric properties. R-P series compounds are represented as $\text{A}_{n+1}\text{B}_n\text{O}_{3n+1}$ for +2 valence state 'A' cations and +4 valence 'B' ions, with C usually being oxygen (-2 valence) [1]. Structurally, they reveal themselves as integral- n ABO_3 perovskite blocks, with inserted AO sheets in-between, along the c -axis. $\text{La}_{1.4}\text{Sr}_{1.6}\text{Mn}_2\text{O}_7$ has been shown to possess inter-planar tunneling induced low-field magneto-resistance [2]. Development of ferromagnetic clustering in the long range antiferromagnetic (AFM) ordering has been reported in $n=3$ R-P compound $\text{La}_{3-x}\text{Sr}_{1+3x}\text{Mn}_3\text{O}_{10}$ [3]. Hybrid improper ferroelectricity (HIF) supported by first-principles calculation has been evident in $n=2$ R-P compound $\text{Ca}_3\text{Ti}_2\text{O}_7$ [4, 5]. Here, the ferroelectric mechanism is described via combination of two octahedral distortion patterns [6]. These distortions offer scope for magneto-electric (ME) coupling and multiferroicity; since unfulfilled d -orbital accommodated in the oxygen octahedra favors (anti)ferromagnetism, which relates profoundly with the metal-oxygen-metal bond angles [7]. Emphasis on $n=2$ R-P system $\text{Ca}_3\text{Mn}_2\text{O}_7$ has been due its expected candidacy for ME coupling [6]. $\text{Ca}_3\text{Mn}_2\text{O}_7$ exhibits structural transition from $I4/mmm$ tetragonal phase to $\text{Cmc}21$ orthorhombic phase, with introduction of octahedral rotation in (001) plane, along with the octahedral tilt about [100] axis [8]. Complementarily, octahedral tilting supports weak ferromagnetism and octahedral rotation induces magneto-electricity [9].

Inversion-symmetry-breaking orthorhombic phase in $\text{Ca}_3\text{Mn}_2\text{O}_7$ can possess ferroelectricity (FE) [6]. Electric field tunability of octahedral rotation is expected to enhance the ME effect. The structural transition covers a wide (300-600K) temperature range [10], with coexistent tetragonal and orthorhombic phases. In pure orthorhombic phase, relaxor behaviour has been suggested [10] below the room temperature. Because of the high leakage-current at high temperatures in the orthorhombic phase, there have been difficulties in experimentally ascertaining ferroelectricity in the system [7]. Upon cooling, dielectric losses get reduced and ferroelectricity with measurable polarization is detected below 60K [10], which can be further explored at lower temperatures. Moreover, magnetic ordering at 123K is expected to affect the dipolar interactions, via the magneto-electric effect. From first-principles calculations [6], Benedek and Fennie have reported G-type AFM ground state for the system, with a net perpendicular spin-canted moment via spin-orbit (S-O) interactions. Dzyaloshinskii's criteria explain the canted moment via the oxygen-octahedral tilt distortion. ME effect for $\text{Ca}_3\text{Mn}_2\text{O}_7$ has been demonstrated by Zhu et. al.

* Corresponding Author: amawasthi@csr.res.in

[11], via measurements of the magnetization under electric field; 6% reduction in magnetization at 4K with the application of E -field of 40 kV/m under 100 Oe H -field has been reported.

It is well known that octahedral rotations have profound effect on transition metal-oxygen-transition metal (TM-O-TM) bond angle, which further affects the interaction between spins [12, 13]. In $\text{Ca}_3\text{Mn}_2\text{O}_7$ system, antiferromagnetic transition with Néel temperature 123K, along with the emergence of weak ferromagnetism (WFM) below 110K, have been reported previously [14]. Dzyaloshinskii-Moriya (D-M) interaction favored WFM clusters' formation in the AFM-matrix, inducing an exchange-bias (EB), was characterized in detail [14, 15], and the magnetic evolution is as summarized in fig.1. In $\text{Ca}_3\text{Mn}_2\text{O}_7$, structural distortions prompt coupling between spin and charge degrees of freedom [9]. Here, we present the linear/non-linear dielectric properties of $\text{Ca}_3\text{Mn}_2\text{O}_7$, and their correlation with magnetic-evolution/phase-mixing is compared & distinguished. Magneto-dielectricity is explored under applied magnetic field, across a sufficiently wide temperature range covering the AFM ordering at $T_N=123\text{K}$.

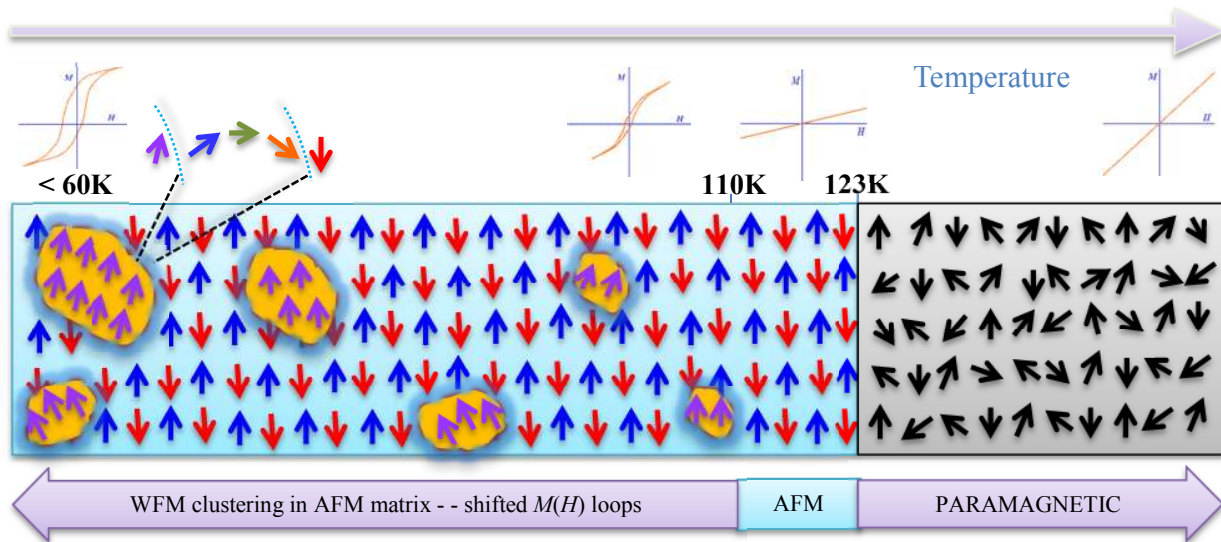


Fig.1. Schematic picturizing the magnetic state evolution in $\text{Ca}_3\text{Mn}_2\text{O}_7$ system with sub-ambient cooling.

RESULTS

Dielectric Spectroscopy:

Low temperature fundamental dielectric response along with second harmonic measurements have been performed in parallel-plate capacitor configuration, from 200K down to 7.5K in the frequency range of 50 Hz to 300 kHz, using NovoControl Alpha-A Broadband Impedance Analyzer. To study the magneto-dielectricity in the system, dielectric measurements under application of magnetic field (H) have also been performed in Oxford NanoSystems Integra 9T magnet-cryostat.

Fig.2(a) presents the dielectric constant $\epsilon'(T)$ of $\text{Ca}_3\text{Mn}_2\text{O}_7$ at various frequencies. Here, sharp frequency-dependent step-change in $\epsilon'(T)$ is observed. At high- T 's, relaxation times $\tau(T)$ are small enough that even at higher radio frequencies (RF) condition $2\pi f\tau(T) < 1$ applies; resulting in a rather small frequency-dependence of $\epsilon'(T)$, as observed.

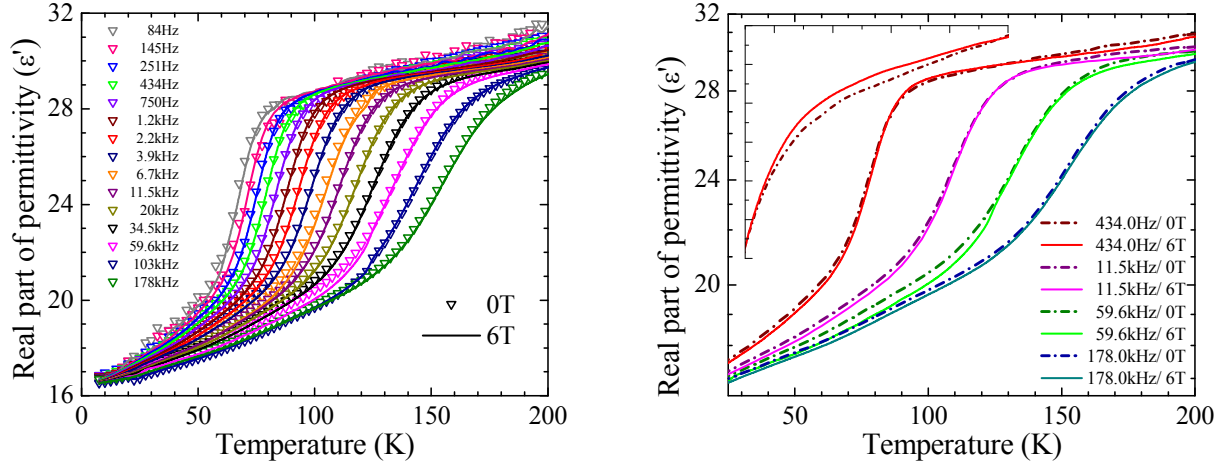


Fig.2 (a): Temperature dependent dielectric constant obtained for different frequencies. (b): $\epsilon'(T)$ at selected frequencies under zero- and 6T magnetic field, depicting change in $\epsilon'(T)$ under the application of H -field.

In layered perovskites, FE-instability consists of O6-octahedron rotations, with negligible off-centering of the B-site cation. The associated energy-gain (due to lattice-strain) and energy-loss (due to dipole-dipole interaction) here rather settle in introducing antiferro-distortive (AFD) -like features over a temperature window [16], thereby suppressing the long-range FE-ordering in the system at a sharp transition temperature [17]. In the quantum paraelectric-like AFD systems, chemical substitution, application of electric field, or dimensional-strain can induce the FE [18]. In the layered $\text{Ca}_3\text{Mn}_2\text{O}_7$, no specific heat anomaly pertaining to a long-range FE transition is observed below the room temperature [11]. At lower temperatures however, magnetic ordering at $T_N=123\text{K}$ supports FE in this magneto-electric system [10].

Appearance of orthorhombic phase upon cooling supports the development of ferroelectric correlations between the dipoles; manifest here as step-like (thermally-activated) decrease of the dielectric constant. Thus-increased $\tau(T)$ leads to resonance of the measurement frequency and the response timescale of the correlated dipoles ($2\pi f\tau(T)=1$); which marks maximum slopes (inflexion-points) of $\epsilon'(T)$, at successively lower frequencies upon cooling. Similar steps in permittivity are discernible in the report by Liu et. al. [10]. Here, the correlations produce size-dispersed dipole-clusters, each responding optimally at different frequency ($\omega_p(T) \sim 1/\text{cluster-size}$), which shows up in thermally activated dielectric spectra. For a given measurement frequency, super-resonance ($2\pi f\tau(T) > 1$) condition upon further cooling causes the roll-off of $\epsilon'(T)$ to lower values, for the same inertial reason as occurs for the $\epsilon'(f)$ -isotherms at high frequencies.

Change in $\epsilon'(T)$ produced under H -field is zoomed-on in fig.2(b), shown at selected frequencies for clarity. At temperatures above the $\epsilon'(T)$ -step, H -field enhances correlations between the dipoles, evident from $\epsilon'(6\text{T}) < \epsilon'(0\text{T})$ (fig.2b). Also, for frequencies $f \geq 11.5$ kHz, at all temperatures $\epsilon'(T)$ simply reduces under the field. At lower frequencies however, H -field alters the dielectric constant in both +ve and -ve sense over different temperature ranges, depending upon the extent of the dipolar interactions. At probing frequencies $f < 11.5\text{kHz}$, H -field mobilizes the larger/frozen dipolar clusters ($2\pi f\tau_{cl} > 1$; $\epsilon'(6\text{T}) > \epsilon'(0\text{T})$) over 80-130K and consolidates/freezes the smaller ones ($2\pi f\tau_{cl} < 1$; $\epsilon'(6\text{T}) < \epsilon'(0\text{T})$) below 80K.

Associated with the step-like change in $\epsilon'(T)$, relaxation peaks in loss tangent ($\tan\delta = \epsilon''/\epsilon'$) are observed, as shown in fig.3(a). Our high-frequency loss-tangent results agree fairly with that presented by Liu et. al. [10]. Increase in the peak temperature of $\tan\delta(T)$ isochrones at higher frequency depicts thermally activated character.

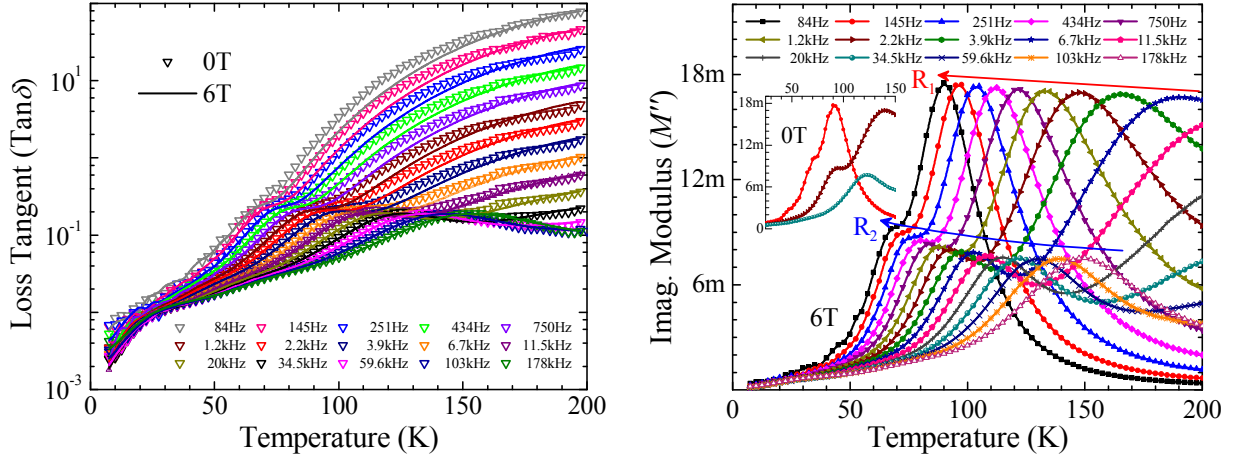


Fig.3 (a): Temperature dependent loss-tangent at different frequencies, under zero- and 6T magnetic field. (b): Modulus $M''(T)$ isochrones under 6T applied H -field at various frequencies, depicting the two relaxations R_1 and R_2 . Inset shows representative isochrones without the H -field.

Neither the dielectric constant nor the loss-tangent indicate any explicit anomalies across the AFM- T_N . For further insight, dielectric modulus ($M^* = 1/\epsilon^* = M' + iM''$) is analyzed, which reveals two sets of localized dipole-relaxations in the system [19]. Figure 3(b) shows imaginary modulus $M''(T)$ at selected frequencies over 90-150K, under zero- (inset) and 6T (main panel) magnetic field. $M''(T)$ isochrones here reveal two relaxation processes in the system; one (R_1) well-developed at lower frequencies with higher modulus— persisting to higher frequencies with increase in temperature— and another (R_2) with comparatively low modulus well-formed at relatively higher frequencies, approximately above 110K.

Frequencies vs. peak-temperature of $M''_f(T)$ has been analyzed to get insight on the interaction among dipoles. (f - T_p) dispersion corresponding to R_1 -relaxations (fig.4(a), zoomed-in over low- T 's) features Arrhenic kinetics [20] at higher temperatures, described by

$$f = f_0 \exp[-E_a/k_B T_p] \quad (1)$$

Here T_p is the temperature corresponding to the M'' -peak at frequency f , E_a is the activation energy for relaxations, f_0 is the approach frequency, and k_B is the Boltzmann constant. However, as our Havriliak-Negami [21] analysis of $M''_f(f)$ spectra has revealed, these peaks are not Lorentzian (broadening parameters $\alpha, \beta < 1$ [9]); Arrhenic kinetics manifest here camouflages non-Debye/liquid-like nature of the dipole-relaxations. For these quasi-independent dipoles, we nominally obtained $E_a^{1A} \sim O(600\text{K})$ and $f_0^{1A}(R_1) \sim O(200 \text{ kHz})$. Enhanced interactions upon cooling manifest Vogel-Fulcher (VFT) dispersion kinetics [22], signifying dipolar-segmentation and their eventual dynamical freezing;

$$f = f_0 \exp[-E_a/k_B(T_p - T_0)] \quad (2)$$

VFT-fit here gives $E_a^{1V}(0\text{T}) = 163.5\text{K}$, $f_0^{1V}(0\text{T}) = 9.64 \text{ kHz}$, and freezing temperature $T_0^1(0\text{T}) = 51.5\text{K}$. Under H -field; $E_a^{1V}(6\text{T}) = 281.8\text{K}$, with $f_0^{1V}(6\text{T}) = 19.1 \text{ kHz}$ and freezing temperature $T_0^1(6\text{T}) = 38.1\text{K}$. Speedup of approach frequencies $\{f_0^{1V}(6\text{T}) > f_0^{1V}(0\text{T})\}$ and reduction of VFT freezing temperature $\{T_0^1(6\text{T}) < T_0^1(0\text{T})\}$ both signify field-suppression of dipole-correlations. This is consistent with magneto-enhancement of the activation-energy barrier $\{E_a^{1V}(6\text{T}) > E_a^{1V}(0\text{T})\}$, which also accompanies thermal fading of dipole-interactions upon warming $\{E_a^{1A} > E_a^{1V}\}$. Magneto-kinetics of R_1 -relaxations thus explains the observed positive magneto-dielectric (MD) effect at lower frequencies.

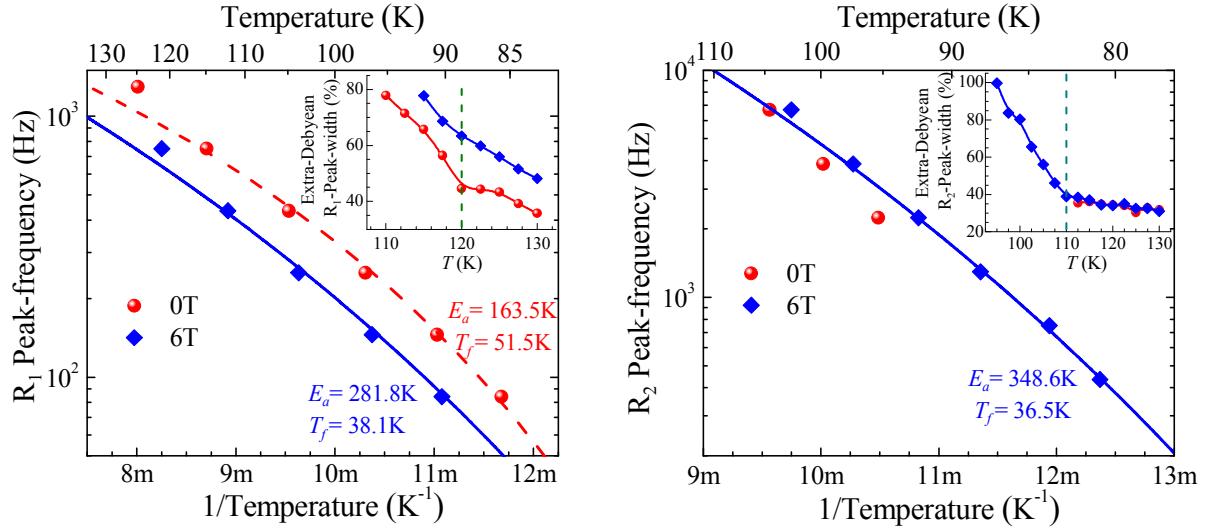


Fig.4(a): Dispersion of the peak frequency $f(1/T_p)$ for R_1 -relaxations. (b): Dispersion of the peak frequency $f(1/T_p)$ for R_2 -relaxations. Insets show the scaled extra-Debye index $\text{SEDI} = [\text{FWHM}/1.14 - 1] \times 100$ of relaxations, marking magnetic evolution at $\sim T_{N,W}$.

R_2 -relaxations in $M''(T)$ replicate those observed in $\tan\delta(T)$; only the peaks occur at slightly higher temperatures [23]. Dispersion kinetics ($f-T_p$) for these relaxations too is Arrhenic at higher temperatures; here also, weakly-interacting ($\alpha, \beta < 1$ [9]) liquid-like degrees of freedom relax quasi-independently, with $E_a^{2A} \sim O(1100\text{K})$ and $f_0^{2A} \sim O(100 \text{ MHz})$. Upon field application, R_2 -relaxation peaks show up down to lower temperatures. Now, the lower- T /field-emergent segmental dynamics (Vogel-Fulcher kinetics) yields $E_a^{2V}(6\text{T}) = 348.6\text{K}$, with $f_0^{2V}(6\text{T}) = 1.14 \text{ MHz}$ and freezing temperature $T_0^2(6\text{T}) = 36.5\text{K}$. Induction of canted-spin WFM-clusters prompts & strengthens local interaction of the site-dipoles undergoing R_2 -relaxations. Emergence of a freezing temperature (otherwise, no $T_0^2(0\text{T})$ here!) signifies purely magneto-actuated consolidation of R_2 -relaxing dipoles, onto which WFM-nanophase gets pinned. In contrast to the R_1 -relaxations, emergence of a finite $T_0^2(6\text{T})$ vs. no $T_0^2(0\text{T})$ reconciles with all-negative magneto-dielectricity at higher frequencies— over which the R_2 -relaxations are observed— as discussed later.

Full width at half maxima (FWHM) have been obtained for the $M''_T(f)$ spectral peaks. FWHM's excess over the constant Debye width is normalized to yield scaled extra-Debye index (SEDI) $= [\text{FWHM}/1.14 - 1] \times 100$, which features an enhanced dynamic range against temperature. Thus obtained $\text{SEDI}_1(T)$ for R_1 -relaxations (fig.4(a)-inset) registers an abrupt-rise anomaly below 120K ($\sim T_N$), marking the magneto-electric segmental-consolidation of correlated dipoles. This anomaly however, smears upon the application of 6T magnetic field as shown, consistent with the high-field reduction and smoothing of the AFM transition temperature. For R_2 -relaxations, $\text{SEDI}_2(T)$ (fig.4(b)-inset) shows a sharp rise below 110K ($\sim T_W$), discernible only under the application of 6T-field. These anomalies are the firstmost (albeit subtle) signatures of the magneto-electric effects, concurring with the system's magnetic evolution. SEDIs uniquely reflect the dynamical heterogeneity in the system's electrical trait— i.e., the distribution of relaxation time $g(\tau)$. Their spectrally-integrated nature implies that the anomalies observed in them have greatly smeared-off/indiscernible bearings in the raw data, measured at individual frequencies, which explains the absence of easily discernible $T_{N,W}$ -signatures in $\epsilon'_T(T)$ (fig.2) and $\tan\delta(T)$ (fig.3).

R_2 (R_1) is recognized to be associated with octahedral-tilts (-rotations), which require higher (lower) activation-energy for the polarization flipping [6]. R_2 -relaxations characterize correlated dipoles which consolidate in wake of the emergent/coupled WFM-nanophase. These field-actuated PNR-segments exhibit dynamical freezing upon further cooling. Observed all -ve MD at higher frequencies is thus entirely traced to the R_2 -relaxations. On the other hand, R_1 -relaxations at lower frequencies (≈ 3.8 kHz) are attributed to the PNR-segments formed in the bulk/AFM-matrix. These larger (slower-responding) entities are somewhat de-correlated under the H -field, accounting for the +ve MD at low-frequencies, over certain temperature window. Thus, the electrical, magnetic, and structural properties in the system are intricately coupled to each other [9].

Magneto-dielectric and Second-harmonic Measurements:

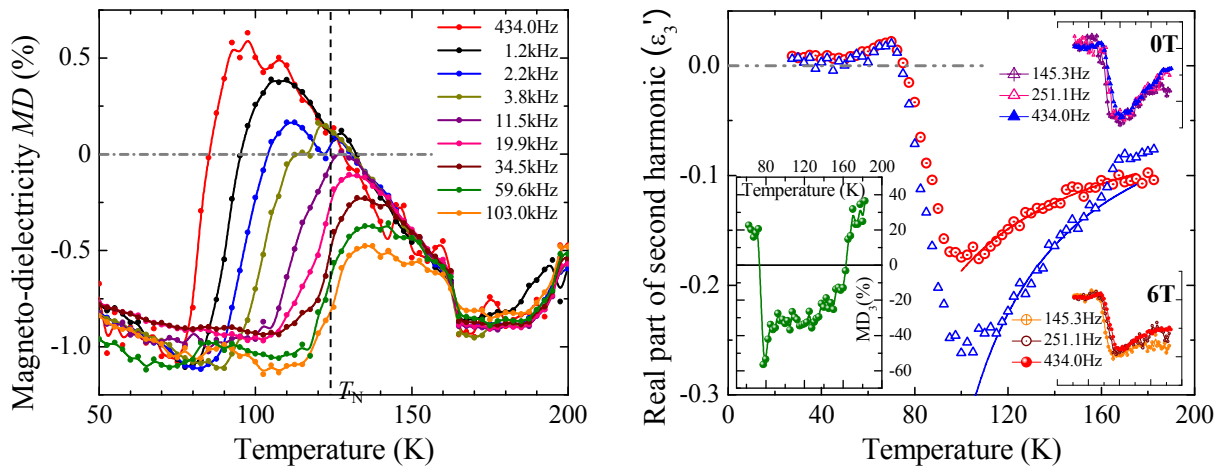


Fig.5(a): Temperature dependence of Magneto-dielectricity MD(%). (b): Temperature dependence of second harmonic (ϵ'_3) signal at 434 Hz, under zero and 6T-magnetic field. Top-right inset: Temperature dependence of ϵ'_3 signal at mentioned frequencies in the absence of H -field; Bottom-right inset: Temperature dependence of ϵ'_3 signal under the application of 6T magnetic field; Left inset: Harmonic magneto-dielectricity $MD_3(\%)$ from the second harmonic signal.

To further correlate electric and magnetic properties of the system, change in dielectric properties with application of 6 Tesla magnetic field has been studied. Figure 5(a) demonstrates temperature dependence of magneto-dielectricity $MD(\%) = \{\epsilon'(H)/\epsilon'(0)-1\} \times 100$, depicting all -ve MD at temperatures above 130K, while at lower temperatures, both negative (high- f 's) and positive (low- f 's) MD can be seen. This is already evident in the zero- and 6T-field $\epsilon'_i(T)$ -plots (fig.2(b)) at selected frequencies. Over 80-130K temperature-window, magnetic field suppresses dipole-interactions in larger clusters (c.f., thermal activation), thereby reducing (increasing) the local polarization (polarizability ϵ'), whereas outside this window, H -field consolidates the growth of smaller-sized dipolar clusters (c.f., thermal de-activation), thereby enhancing (reducing) the local polarization (ϵ'). The dual (\pm ve) nature of MD shows up over the temperature region where consolidating dipolar clusters evolve. The exclusive orientational-liquid at high- T 's however features only -ve MD (i.e., field-enhanced dynamical correlations), as indeed expected.

The counterintuitive 'de-correlating effect' of the applied magnetic field in the intermediate temperature range is driven by the same free-energy considerations, that favor the emergence of isolated WFM nanophase (coexistent with the AFM-matrix) versus phase-separated or uniformly spin-canted configurations. In $M''(T)$ (fig.3(b)), R_2 -relaxation peaks observed without field only above 110K, get extended under 6T

field down to 95K. Evidently, the H -field magneto-electrically enhances the correlations, causing segmentation of the orientational-liquid undergoing the R_2 -relaxations. Thus, 100x faster R_2 -relaxations reasonably admit to a 2-D extent of WFM nano-phase pinned onto the R_2 -relaxations site, vs. the 3-D character of the PNRs in the bulk-AFM, undergoing the slower R_1 -relaxations. Negative-MD from locally more conducting WFM-regions versus the positive-MD traced to the evidently less-conductive AFM-matrix therefore endows a topological attribute to magneto-electricity in this layered compound. Finite MD $\neq 0$ below the VFT- T_0 's signifies the existence of ME-actuated intra-cluster dipole-dynamics. Dual character of magneto-dielectric coupling observed here, associated with the AFM (mostly +ve MD) and WFM (all -ve MD) magnetic sub-phases, duly correlates with the field-suppression of AFM-order ($T_N(6T) < T_N(0T)$) and field-enhancement of WFM ($T_W(6T) > T_W(0T)$) [15].

The magneto-electric effect coupled through structural distortions collaterally manifests in the second-harmonic (ϵ'_3) measurements. Negative-definite $\epsilon'_3(T)$ -signal has been observed, undergoing through an extremum at $\sim 100K$, and vanishing near $\sim 50K$, as shown in fig.5(b). This is in agreement with theoretical modeling for relaxor-like ferroelectrics, exhibiting frequency-dispersive relaxation [24, 25]. The low strength of ϵ'_3 -signal indicates its major contribution from the term $\sim -\chi_1^4$, denoting cluster-induced relaxor-like FE, and not from the bulk polarization term $\sim P^2\chi_1^5$ [25, 26]. Well-measurable second-harmonic signal precisely registers the dynamical transit from the weakly-interacting orientational liquid (Arrhenic dispersion; manifest as the higher- T tail in the ϵ'_3 -signal) to the segmented ones (Vogel-Fulcher kinetics; sharp reduction in the ϵ'_3 -signal below $\sim 100K$). The segmented dipolar interactions evolve upon further cooling and freeze by $\sim 50K$, below which the harmonic signal ϵ'_3 too vanishes. Dispersive $\epsilon'(T)$ vs. relatively dispersion-free $\epsilon'_3(T)$ refer their origins to different (voluminous and aerial, say) topologies, harboring distinct electrical organizations (usual & hyper polarizations, [25]). Specifically, linear (harmonic) signals here likely arise from within (outside) the bulk of the correlated PNR-segments. The extremum in $\epsilon'_3(T)$ around $\sim 100K$ signifies optimum electrical non-linearity.

Increase of harmonic signal upon cooling is expected to diverge critically, with power-law T -dependence [27, 28]

$$|\epsilon'_3| \propto (T - T_g)^{-\gamma} \quad (3)$$

From the fits of $\epsilon'_3(T, H)$ -signals over 115-160K with eq.(3) (solid curves in fig.5(b) main panel), we obtain $T_g(0T) = 53.63K$ as the freezing temperature with divergence exponent $\gamma(0T) = 1.21$ at zero-field—comparing well with $\gamma = 1.25$ found for BTZ35 by Kleemann et. al. [29]— and $T_g(6T) = 40.66K$ with $\gamma(6T) = 0.79$ at 6T-field. The agreement (up to $\sim 5\%$) between the T_g 's and the Vogel-Fulcher T_0 's for the R_1 -relaxations is rather excellent. Together with $T_g(0T, 6T) \approx T_0^1(0T, 6T)$, concurrency of the finite & -ve harmonic MD₃(%) = $\{\epsilon'_3(H)/\epsilon'_3(0) - 1\} \times 100$ over roughly the same temperature-window with the +ve fundamental MD, associates them both to the PNR-segments undergoing R_1 -relaxations; allied with octahedral-rotations, in the bulk/AFM-matrix. Cluster-glassy/power-law critical-divergence of $\epsilon'_3(T)$ versus the relaxor-like/VFT $\tau(T)$ -divergence obtained from $M''(T)$ complementarily corroborate the inter-/intra-PNR origins of the harmonic/fundamental responses, as characterized. Higher e -moments (say, quadru-&octu-poles) can emerge from the vortex-configuration of the dipole-orientations, in the spatially-separated interstices formed by the surrounding PNRs; providing the required non-linear susceptibility in the e -disordered/zero- P phase of the system, apparently responsible for the observed harmonic ϵ'_3 -signal.

Harmonic signal is H -dependent and exists ($\epsilon'_3(T, H) \neq 0$) only down to the freezing temperature $\sim 50\text{K}$ of the segmented dynamics; yielding $\text{MD}_3 \neq 0$ over the T -window hosting dynamically-activated dipoles. Over $80\text{-}160\text{K}$, $\epsilon'_3(T)$ -signal decreases under the applied H -field, giving -ve MD_3 . Expectedly, under-field decorrelation of dipoles relaxing at low-frequencies (yielding $\text{MD} > 0$) also thermally randomizes the ‘higher-moments’ in the PNR-interstices; thereby decreasing the harmonic response. This is complemented by the magnitude-crossing of the zero-field and in-field ϵ'_3 -signals at 434Hz roughly across $\sim 160\text{K}$, above which +ve MD_3 (fig.5(b)-left inset) now concurs with the -ve MD (fig.5(a)). Vis-à-vis observed $\text{MD}(<T_0) \neq 0$ from the ‘frozen’ PNRs, both $\epsilon'_3(<T_0)$ & $\text{MD}_3(<T_0) \approx 0$ (\equiv data-scatter) further corroborate the (magneto-)harmonic response being exterior to the PNR-segments, besides non-contributed to by (even local) $P^2\chi_1^5$ -terms. Under-field enhancement of T_W and actuation of (R_2 -relaxing) PNR-segments also suggests the localization of WFM-nanophase at the PNR₂-interstices; although further work and supportive observations are mandated to rigorously establish the circumstance.

CONCLUSIONS

Magneto-dielectric coupling in $\text{Ca}_3\text{Mn}_2\text{O}_7$ has been established in reference to two structural distortions—octahedral-tilt and octahedral-rotation. We have analyzed the signatures of interacting-dipole structures, featuring vitreous relaxation kinetics upon cooling below the AFM transition and with the emergence of weak ferromagnetic nano-phase at $T_W \sim 110\text{K}$, in the AFM matrix ($T_N = 123\text{K}$). Alterations of dipoles’ correlation-status are allied with the system’s magnetic evolution and reflect in the magneto-dielectric signals, upon magnetic field application. Observed second-harmonic magneto-dielectricity is some two orders of magnitude larger, vis-à-vis that obtained in the fundamental response. Vortex-configuration of dipoles’ orientation in the PNR-interstices is invoked as the source of the harmonic electrical response, consistent with its observed characteristics. Structural, magnetic, and electrical coupling in this Ruddlesden-Popper compound is the consequence of its layered structure, which is found to exhibit a topological character. Hence, the ME-coupling can be tailored in its thin-film or nano-fiber formations, where the exclusive features can be enhanced/suppressed by dimensional reduction and intrinsic strain. Furthermore, chemically-doped variants may be investigated to tune the magneto-electric functionality.

ACKNOWLEDGMENTS

Suresh Bhardwaj is thankfully acknowledged for his technical help and facilitation of the measurements.

REFERENCES

1. Beznosikov, B.V. and Aleksandrov, K.S. (2000). Perovskite-like crystals of the Ruddlesden-Popper series. *Crystallography Reports* **45**(5), 792-798.
2. Kimura, T., Tomioka, Y., Kuwahara, H., Asamitsu, A., Tamura, M., and Tokura, Y. (1996). Inter-plane tunneling magnetoresistance in a layered manganite crystal. *Science* **274**(5293), 1698-1701.
3. Tang, Y.K., Ma, X., Kou, Z.Q., Sun, Y., Di, N.L., Cheng, Z.H., and Li, Q.A. (2005). Slight La doping induced ferromagnetic clusters in layered $\text{La}_{3-3x}\text{Sr}_{1+3x}\text{Mn}_3\text{O}_{10}$ ($x=1.00, 0.99, 0.95$). *Physical Review B* **72**(13), 132403.
4. Mulder, A.T., Benedek, N.A., Rondinelli, J.M., & Fennie, C.J. (2013). Turning ABO_3 Antiferroelectrics into Ferroelectrics: Design Rules for Practical Rotation-Driven Ferroelectricity in Double Perovskites and $\text{A}_3\text{B}_2\text{O}_7$ Ruddlesden-Popper Compounds. *Advanced Functional Materials* **23**(38), 4810-4820.
5. Oh, Y.S., Luo, X., Huang, F.T., Wang, Y., and Cheong, S.-W. (2015). Experimental demonstration of hybrid improper ferroelectricity and the presence of abundant charged walls in $(\text{Ca}, \text{Sr})_3\text{Ti}_2\text{O}_7$ crystals. *Nature Materials* **14**(4), 407.
6. Benedek, N.A. and Fennie, C.J. (2011). Hybrid improper ferroelectricity: a mechanism for controllable polarization-magnetization coupling. *Physical Review Letters* **106**(10), 107204.
7. Liu, X.Q., Wu, J.W., Shi, X.X., Zhao, H.J., Zhou, H.Y., Qiu, R.H., Zhang W.Q., and Chen, X.M. (2015). Hybrid improper ferroelectricity in Ruddlesden-Popper $\text{Ca}_3(\text{Ti}, \text{Mn})_2\text{O}_7$ ceramics. *Applied Physics Letters* **106**(20), 202903.
8. Harris, A.B. (2011). Symmetry analysis for the Ruddlesden-Popper systems $\text{Ca}_3\text{Mn}_2\text{O}_7$ and $\text{Ca}_3\text{Ti}_2\text{O}_7$. *Physical Review B* **84**(6), 064116.
9. Sahlot, P., Sharma, G., Sathe, V.G., Sinha, A.K., and Awasthi, A.M. (2019). Interplay of Spin, Lattice, Vibration, and Charge Degrees of Freedom in $\text{Ca}_3\text{Mn}_2\text{O}_7$. Preprint arXiv:1903.05995.
10. Liu M., Zhang Y., Lin L.F., Lin L., Yang S., Li X., Wang Y., Li S., Yan Z., Wang X., Li X.G., Dong S., and Liu J.M. (2018). Direct observation of ferroelectricity in $\text{Ca}_3\text{Mn}_2\text{O}_7$ and its prominent light absorption. *Applied Physics Letters* **113**(2), 022902.
11. Zhu, W., Pi, L., Huang, Y., Tan, S., and Zhang, Y. (2012). Electrically induced decrease of magnetization in $\text{Ca}_3\text{Mn}_2\text{O}_7$. *Applied Physics Letters* **101**(19), 192407.
12. Benedek, N.A., Mulder, A.T., and Fennie, C.J. (2012). Polar octahedral rotations: a path to new multifunctional materials. *Journal of Solid State Chemistry* **195**, 11-20.
13. Goodenough, J.B. (1955). Theory of the role of covalence in the perovskite-type manganites $[\text{La}, \text{M}(\text{II})] \text{MnO}_3$. *Physical Review* **100**(2), 564.
14. Sahlot, P., Jana, A., and Awasthi, A.M. (2018). Exchange bias in multiferroic $\text{Ca}_3\text{Mn}_2\text{O}_7$ effected by Dzyaloshinskii-Moriya interaction. *AIP Conference Proceedings* **1942** (No. 1) 130009.
15. Sahlot, P. and Awasthi, A.M. (2019). Uncompensated-spins Induced Weak Ferromagnetism and Magneto-conductive Effects in $\text{Ca}_3\text{Mn}_2\text{O}_7$. Preprint arXiv:1901.04778.
16. López-Pérez, J. and Íñiguez, J. (2011). Ab-initio study of proper topological ferroelectricity in layered perovskite $\text{La}_2\text{Ti}_2\text{O}_7$. *Physical Review B*, **84**(7), 075121.
17. Zhong, W. and Vanderbilt, D. (1995). Competing structural instabilities in cubic perovskites. *Physical Review Letters* **74**(13), 2587.
18. Sai, N. and Vanderbilt, D. (2000). First-principles study of ferroelectric and antiferrodistortive instabilities in tetragonal SrTiO_3 . *Physical Review B* **62**(21), 13942.
19. Gerhardt, R. (1994). Impedance and dielectric spectroscopy revisited: distinguishing localized relaxation from long-range conductivity. *Journal of Physics and Chemistry of Solids* **55**(12), 1491-1506.

20. Menzinger, M. and Wolfgang, R. (1969). The meaning and use of the Arrhenius activation energy. *Angewandte Chemie International Edition in English* **8**(6), 438-444.
21. Havriliak, S., & Negami, S. (1966). A complex plane analysis of α -dispersions in some polymer systems. *Journal of Polymer Science Part C: Polymer Symposia* **14**(1), 99-117.
22. Tagantsev, A.K. (1994). Vogel-Fulcher relationship for the dielectric permittivity of relaxor ferroelectrics. *Physical Review Letters* **72**(7), 1100.
23. Cao, W. and Gerhardt, R. (1990). Calculation of various relaxation times and conductivity for a single dielectric relaxation process. *Solid State Ionics* **42**(3-4), 213-221.
24. Pirc, R. and Blinc, R. (1999). Spherical random-bond-random-field model of relaxor ferroelectrics. *Physical Review B* **60**(19), 13470.
25. Miga, S., Dec, J., and Kleemann, W. (2011). Non-linear dielectric response of ferroelectrics, relaxors and dipolar glasses. In *Ferroelectrics- Characterization and Modeling* (Ed. Mickaël Lallart, InTech). ISBN 978-953-307-455-9.
26. Ikeda, S., Kominami, H., Koyama, K., and Wada, Y. (1987). Nonlinear dielectric constant and ferroelectric-to-paraelectric phase transition in copolymers of vinylidene fluoride and trifluoroethylene. *Journal of Applied Physics* **62**(8), 3339-3342.
27. Binder, K. and Reger, J.D. (1992). Theory of orientational glasses: models, concepts, simulations. *Adv. Phys.* **41**(6), 547-627.
28. Pirc, R., Tadić, B., and Blinc, R. (1994). Nonlinear susceptibility of orientational glasses. *Physica B: Condensed Matter* **193**(2), 109-115.
29. Kleemann, W., Miga, S., Dec, J., and Zhai, J. (2013). Crossover from ferroelectric to relaxor and cluster glass in $\text{BaTi}_{1-x}\text{Zr}_x\text{O}_3$ ($x=0.25-0.35$) studied by non-linear permittivity. *Appl. Phys. Lett.* **102**, 232907.